ADVANCED MATERIALS

Supporting Information

Emergent Magnetic States and Tunable Exchange Bias at 3d Nitride Heterointerfaces

Qiao Jin, Qinghua Zhang, He Bai, Amanda Huon, Timothy Charlton, Shengru Chen, Shan Lin, Haitao Hong, Ting Cui, Can Wang, Haizhong Guo, Lin Gu, Tao Zhu, Michael R. Fitzsimmons, Kui-juan Jin,* Shanmin Wang,* and Er-Jia Guo*

Supplementary Materials for

# Emergent magnetic states and tunable exchange bias at 3*d* nitride heterointerfaces

Qiao Jin, Qinghua Zhang, He Bai, Amanda Huon, Timothy Charlton, Shengru Chen, Shan Lin, Haitao Hong, Ting Cui, Can Wang, Haizhong Guo, Lin Gu, Tao Zhu, Michael R. Fitzsimmons, Kui-juan Jin,* Shamin Wang,* and Er-Jia Guo*

*Corresponding author. Email: kjjin@iphy.ac.cn , wangsm@sustech.edu.cn, and ejguo@iphy.ac.cn

This PDF file includes:

Supplementary Materials

    Figures S1-S9
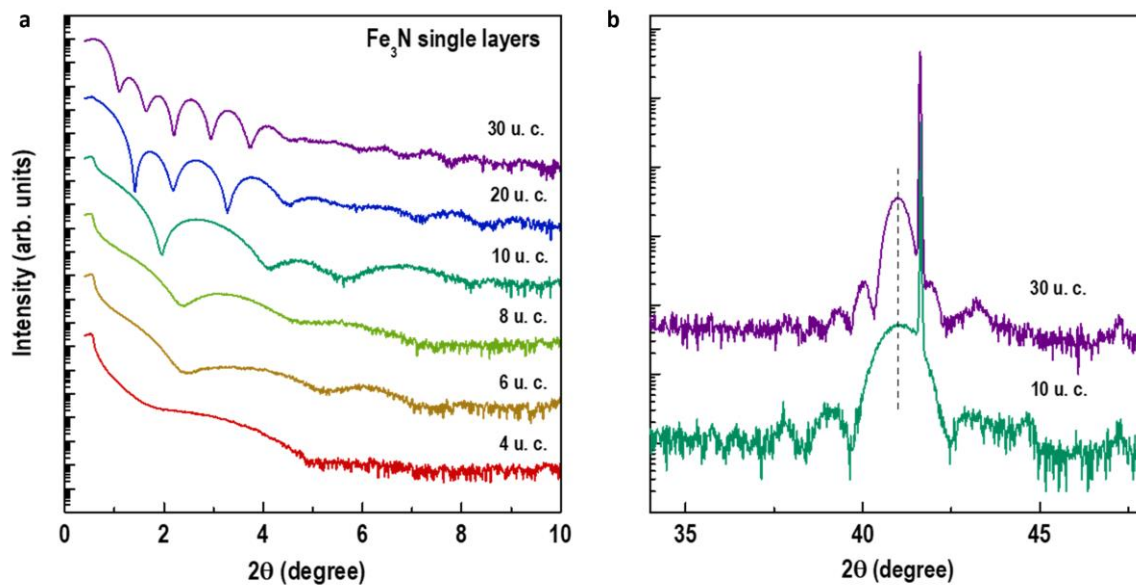
Figure S1. (a) X-ray reflectivities and (b) XRD θ-2θ scans of Fe₃N single layers. The thicknesses of Fe$_3$N single layers, the roughness of film surface and interface are determined from fitting X-ray reflectivity curves using GenX software. The typical roughness of sample's surface is ~ 4 Å, which is comparable to the lattice parameter of Fe$_3$N. (b) XRD θ-2θ scans of Fe3N thin films with thicknesses of 10 and 30 u. c., from which we could find that the out-of-plane lattice constant (~ 4.38 Å) does not change much as the film thickness reducing. This fact maybe caused by the formation of transition layer, resulting in the partial release of epitaxial strain.
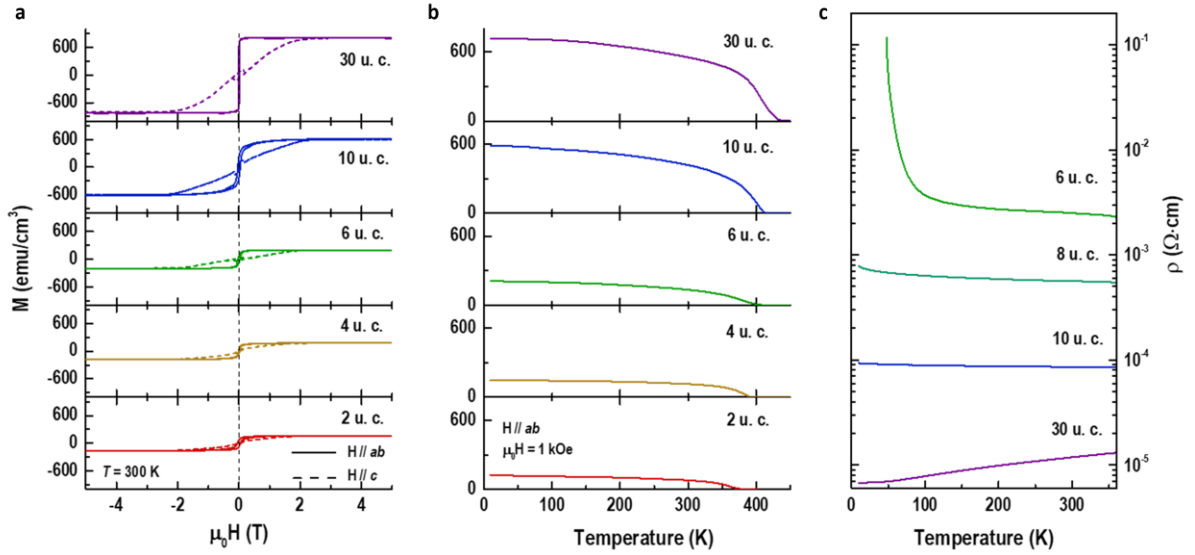
Figure S2. Thickness dependent magnetization and resistivity of Fe₃N single layers. (a) Field-dependent room-temperature magnetization of Fe₃N single layers with a thickness ranging from 2 to 30 u. c. The magnetic easy-axis of Fe₃N films is along the in-plane direction. The saturation moment reduces as increasing the layer thickness. (b) Temperature dependent magnetization of Fe₃N single layers with different film thickness. All measurements were performed along the in-plane direction during the sample warming up and under a magnetic field of 1 kOe. The T_C decreases as reducing the layer thickness. The T_C of a 2-u.c.-thick Fe₃N is ~ 385 K, which is well above the room-temperature. (c) Temperature dependent resistivity of Fe₃N single layers. For a 30-u.c.-thick Fe₃N, the room-temperature resistivity is ~ 11.6 μΩ·cm, which is close to its bulk value of 9.5 μΩ·cm. The Fe₃N single layers undergo a metal-to-insulator transition (MIT) as reducing the layer thickness. The critical thickness for MIT is ~ 8 u.c. The resistivity of Fe₃N is out of the measuring range when its thickness below 4 u. c., indicating a highly insulating state.
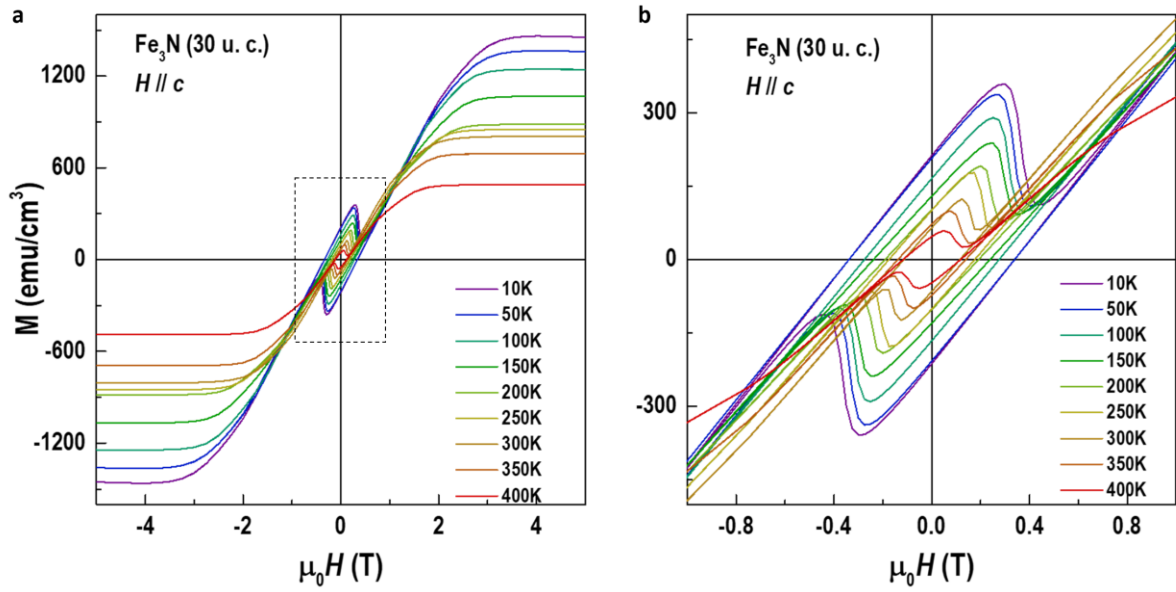
Figure S3. Field-dependent out-of-plane magnetization of a 30-u.c.-thick Fe₃N single layer at various temperatures. The saturation moment reduces gradually as increasing temperature. (b) The zoom-in region in *M-H* loops [dashed rectangle area marked in (a)]. We notice that an abnormal enhancement in the magnetization at low magnetic fields. The switching field and remnant magnetization reduce as increasing temperature. We believe this anomaly may attribute to the sudden realignment of magnetic domains towards the out-of-plane direction.
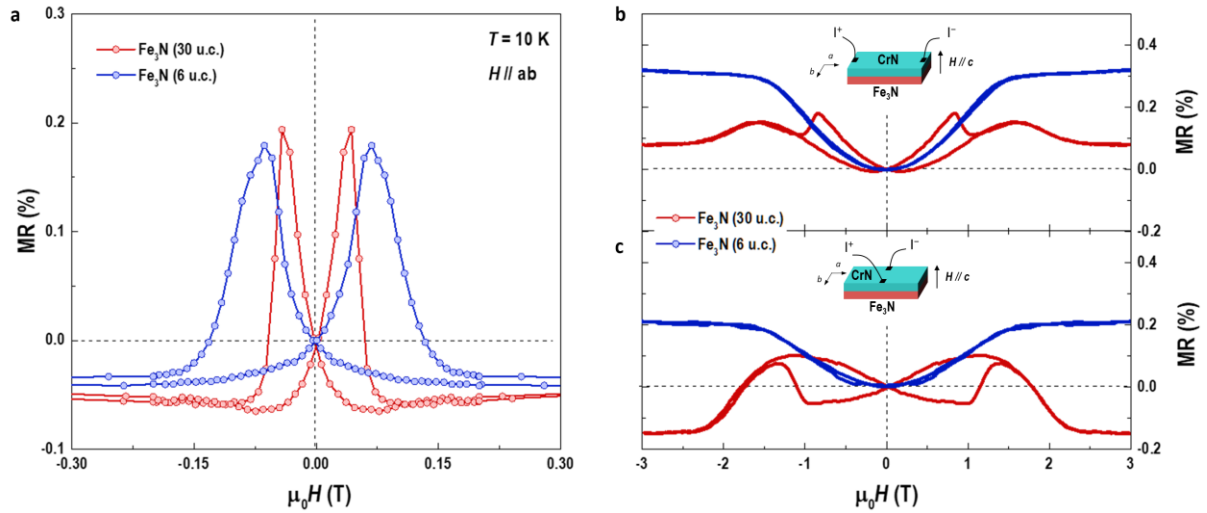
Figure S4. Direct comparison of magnetoresistance (MR) of 6-u.c.- and 30-u.c.-thick Fe₃N single layers. (a) MR at 10 K when $H \,/\!/\, ab$. As reducing the layer thickness, the coercive field increases. The trend of MR as a function of magnetic field is quite similar. (b) and (c) MR at 10 K when $H \,/\!/\, c$ while $I \,/\!/\, a$ and $I \,/\!/\, b$, respectively. For a 30-u.c.-thick Fe₃N layer, MR ($I \,/\!/\, a$) exhibits a batman-like shape with positive MR under magnetic fields and reaches a maximum value at the coercive fields. While, the majority of MR ($I \,/\!/\, b$) shows negative values, in sharp contrast to those values when $I \,/\!/\, a$. The oppositive behavior indicates the asymmetric in-plane magnetic ground states in the thick Fe₃N films. For a 6-u.c.-thick Fe₃N single layer, the MR ($I \,/\!/\, a$) is nearly identical to the MR ($I \,/\!/\, b$), suggesting the in-plane magnetic asymmetry breaks when the thickness of Fe₃N layers approaches to its two-dimensional limit.
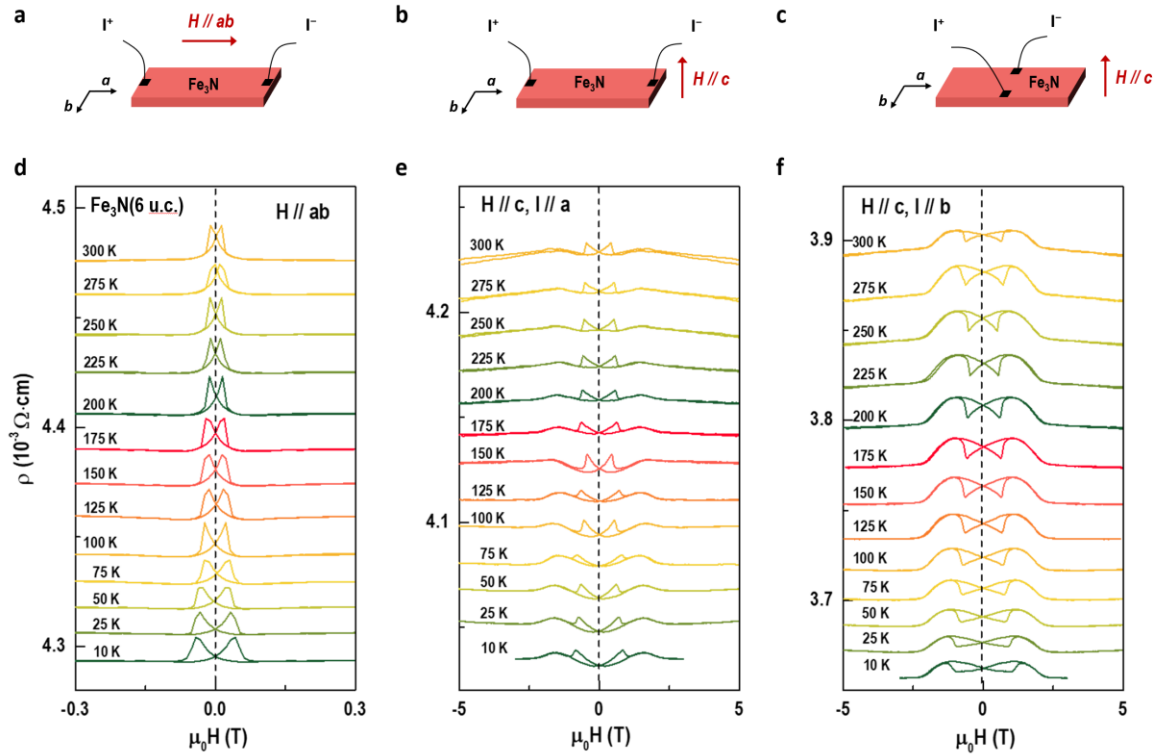
Figure S5. Magnetoresistance of a 6-u.c.-thick Fe₃N single layer. (a)-(c) Schematics of measuring setups, in which the directions of magnetic fields and applied currents are marked clearly. (d)-(f) Magnetoresistance of a 6-u.c.-thick Fe₃N single layer at various temperatures. The transport measurements were taken following the geometries of setups above each MR curves.
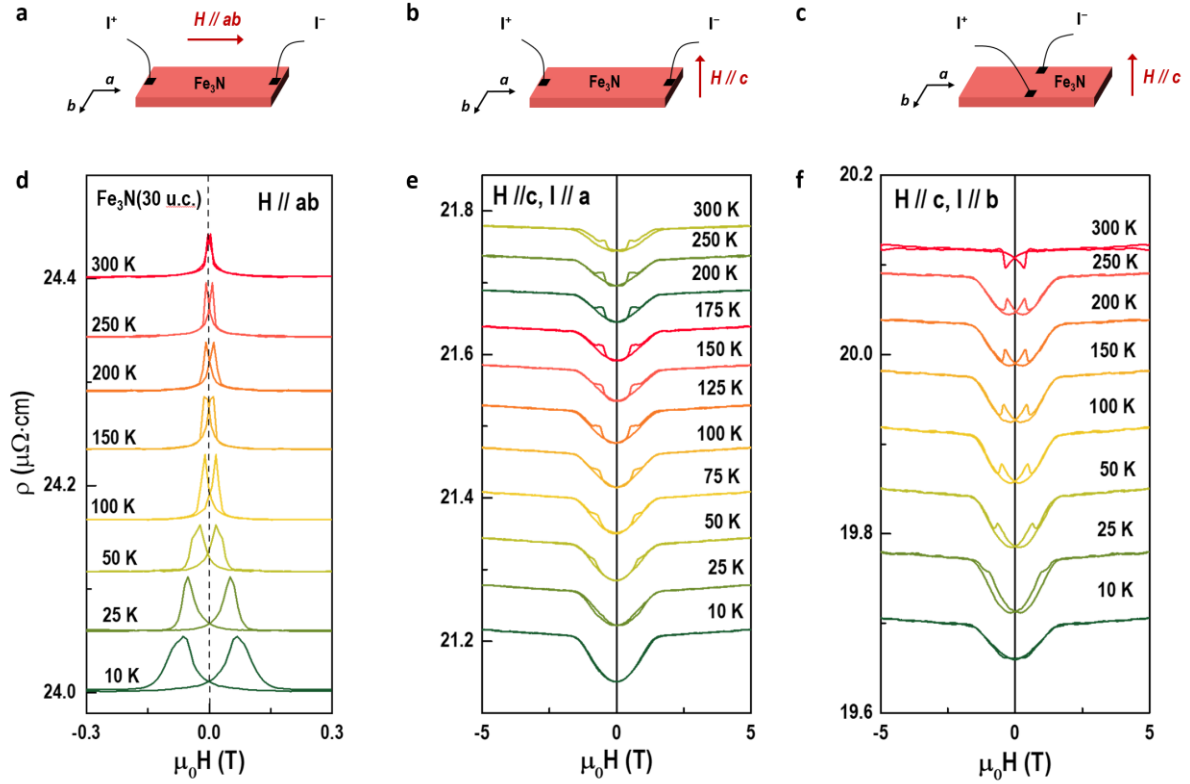
Figure S6. Magnetoresistance of a 30-u.c.-thick Fe₃N single layer. (a)-(c) Schematics of measuring setups, which is the same as those in Figure S5. (d)-(f) Magnetoresistance of a 30-u.c.-thick Fe₃N single layer at various temperatures. The transport measurements were taken following the geometries of setups above each MR curves.
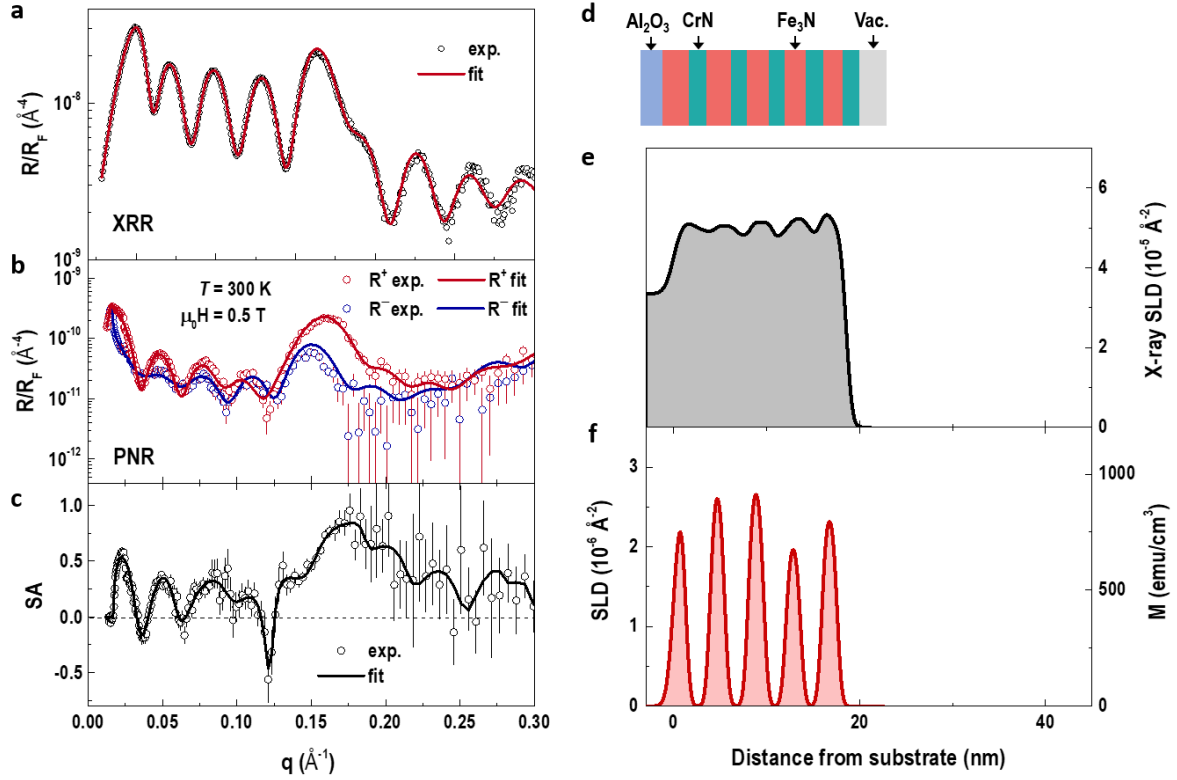
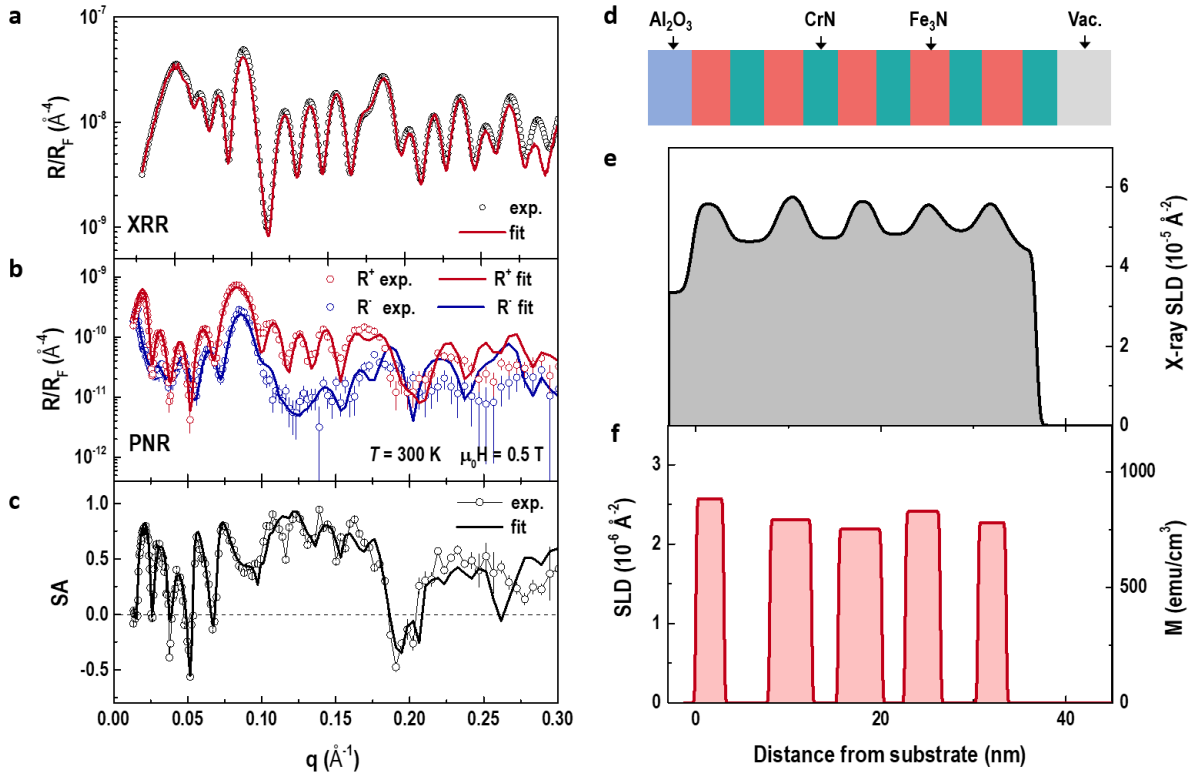**Figure S7. Chemical and magnetization depth profiles of a [(CrN)₅/(Fe₃N)₅]₅ superlattice**.
(a) X-ray reflectivity of the superlattice. (b) Neutron reflectivities from spin-up (red, R^+) and spin-down (blue, R^-) polarized neutrons. The measurements were taken at room temperature under a magnetic field of 0.5 T. The large splitting between R^+ and R^- suggests large net magnetic moment across the entire sample. The spin asymmetry (SA) is calculated by $(R^+-R^-)/(R^++R^-)$. Open symbols and solid lines are experimental data and best fits, respectively. To fit the neutron reflectivity, we use a fixed chemical profile obtained from X-ray reflectivity fitting and then the magnetization of each layer can be obtained precisely. (d) Schematic of a sample structure. The alternative CrN and Fe₃N layers with a thickness of 5 u. c. repeat five times and grown on a Al₂O₃ substrate. (e) and (f) Chemical and magnetization depth profiles, respectively. The atomic density of Fe₃N is slightly larger than that of CrN. We observe an averaged magnetization of ~ 730 emu/cm³ in Fe₃N layers, while the CrN layers exhibit negligible moment, suggesting that the CrN layers maintain their antiferromagnetic character.

Figure S8. Chemical and magnetization depth profiles of a [(CrN)$_{10}$/(Fe$_3$N)$_{10}$]$_5$ superlattice. (a) and (b) X-ray and neutron reflectivities, respectively. All measurements were taken at room temperature. The PNR measurements were performed under a magnetic field of 0.5 T. To fit the neutron reflectivity, we use the chemical profiles, including the layer thickness and roughness, obtained from X-ray reflectivity. Fittings in this manner could obtain the magnetization of each layer precisely. (c) Calculated spin asymmetry. The open symbols and solid lines are the experimental data and best fits, respectively. (d) Schematic of sample structure. (e) and (f) Chemical and magnetization profiles of a [(CrN)$_{10}$/(Fe$_3$N)$_{10}$]$_5$ superlattice. The obtained averaged magnetization of Fe$_3$N layer is ~ 760 emu/cm^3, while that of CrN is zero, indicating an antiferromagnetic nature.
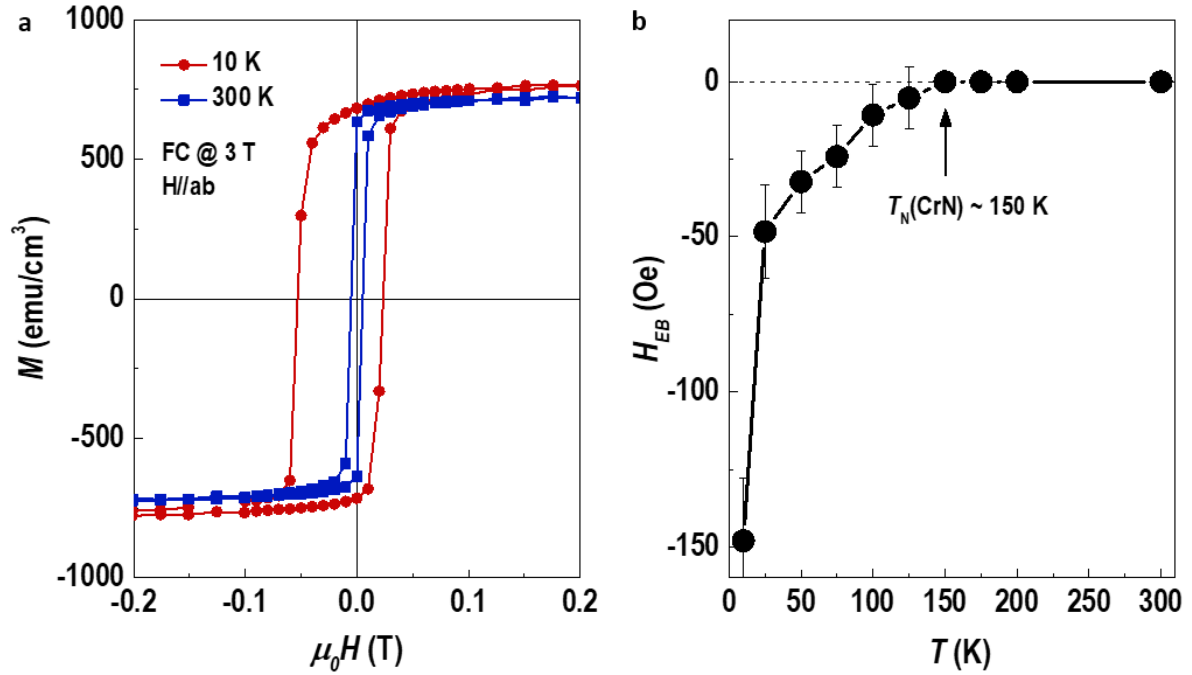
Figure S9. Magnetic loops and temperature dependence of exchange bias field. (a) Magnetization-field loops at 10 and 300 K for a CrN/Fe_3N membrane after field-cooling from room-temperature in a 3 T field. Clearly, the magnetic loop at 10 K shifts to negative field while the loop shift is negligible small at 300 K, as is evident from the superposition of the field-cooled loop. (b) Corresponding temperature dependence of H_{EB} after the same cooling process. The magnetic field was applied parallel to the plane of the sample. The H_{EB} reduces to zero when the CrN film undergoes an antiferromagnetic to paramagnetic phase transition (Neél temperature, T_N) at ~ 150 K. This behavior has been reported in our previous works. The error bars are derived from the uncertainty in the values of the H_C due to the finite number of the data points in the magnetic loops.